The Astronomical Journal, 123:2110–2120, 2002 April

PHYSICAL PROPERTIES OF TRANS-NEPTUNIAN OBJECT (20000) VARUNA

David C. Jewitt and Scott S. Sheppard
Institute for Astronomy, University of Hawaii, 2680 Woodlawn Drive, Honolulu, HI 96822; jewitt@ifa.hawaii.edu, sheppard@ifa.hawaii.edu
Received 2001 November 13; accepted 2002 January 7

ABSTRACT

We present new time-resolved photometric observations of the bright trans-Neptunian object (20000) Varuna and use them to study the rotation period, shape, and color. In observations from 2001 February and April, we find a best-fit two-peaked light curve with period 6.3442 ± 0.0002 hr. The peak-to-peak photometric range in the R band is 0.42 ± 0.02 mag. We find no rotational variation in colors over the $0.45\ \mu\text{m} \leq \lambda \leq 0.85\ \mu\text{m}$ wavelength range. From the short, double-peaked period and large amplitude, we suggest that Varuna is an elongated, body, perhaps close in shape to one of the Jacobi ellipsoids. If so, the ratio of the axes projected into the plane of the sky is 1.5:1 and the density is near 1000 kg m^{-3}. Varuna may be a rotationally distorted rubble pile, with a weak internal constitution due to fracturing by past impacts. The high specific angular momentum implied by our observations and recent detections of binary trans-Neptunian objects both point to an early, intense collisional epoch in which large trans-Neptunian objects were $\sim$100 times more abundant than now. In order to maintain a cosmochemically plausible rock : ice mass ratio of $\sim$0.5, Varuna must be internally porous.

Key words: Kuiper belt — minor planets, asteroids — Oort cloud — solar system: general

1. INTRODUCTION

The trans-Neptunian objects (TNOs) have semimajor axes larger than that of Neptune (Jewitt & Luu 2000) and are thought to be the products of arrested growth in the tenuous outer parts of the accretion disk of the sun (Kenyon & Luu 1999). Their large mean heliocentric distances and resulting low surface temperatures suggest that they may retain a substantial volatile fraction. Indeed, the trans-Neptunian region is widely held to be the source of the ice-rich nuclei of short-period (specifically Jupiter-family) comets. In this sense, the TNOs are repositories of some of the solar system's least evolved, most primitive material. There is widespread interest in the physical (and chemical) properties of these bodies. Unfortunately, most known TNOs are too faint to permit easy investigation, even with the largest available telescopes. For this reason, the bright TNO (20000) Varuna (apparent red magnitude $\sim$19.7) has already attracted considerable observational attention.

Varuna was discovered on 2000 November 28 and given the provisional designation 2000 WR106 (McMillan & Larsen 2000). Prediscovery observations from 1955 were soon uncovered (Knofel & Stoss 2000), leading to the accurate determination of the orbit and the classification as a "classical TNO" (Jewitt & Luu 2000), with semimajor axis 43.274 AU, inclination 17°.1, and eccentricity 0.056. Simultaneous thermal and optical observations yield red geometric albedo $p_R = 0.07^{+0.030}_{-0.017}$ and equivalent circular diameter 900^{+129}_{-145} km (Jewitt, Aussel, & Evans 2001). Varuna is currently one of the largest known trans-Neptunian objects and is comparable in size to the largest main-belt asteroid, 1 Ceres. Farnham (2001) reported a rotational light curve from observations taken 2001 January 24–27, with a single-peaked period of 3.17 hr and "amplitude" of 0.5 mag. Farnham also found other plausible periods, including 2.78 and 3.67 hr. Motivated by this remarkable result, we immediately undertook observations to secure an independent determination of the light curve and to search for rotational color variations. Such variations are predicted by the impact-resurfacing model (Luu & Jewitt 1996). In this paper we discuss Varuna's light curve, possible causes of the brightness variations, and what this object may reveal about the collisional environment in the young trans-Neptunian belt.

2. OBSERVATIONS

Optical observations were taken UT 2001 February 17–21 and April 22, 24, and 25 at the University of Hawaii 2.2 m telescope atop Mauna Kea, Hawaii. We used a Tektronix 2048×2048 pixel charge-coupled device (CCD) with a 0".219 pixel^{-1} image scale and a 7' field of view. Images were secured through standard broadband *BVRI* filters based on the Johnson-Kron-Cousins system. The CCD bias level was determined from an overclocked region of the chip. Flat-field calibration was obtained, using a mixture of images of the twilight sky with data frames. The image quality (including contributions from the telescope, wind shake, and atmosphere) varied from 0".6 to 1".2 FWHM, but was mostly concentrated near a mean at 0".7. Absolute calibration of the data was obtained through repeated observations of standard stars from the list by Landolt (1992). The position of Varuna was dithered over the detector to prevent pathological problems in the photometry associated with bad pixels. Images photometrically affected by proximity to bad pixels or field stars and galaxies (including all those from UT 2001 February 21), were rejected from further analysis.

For the purposes of light curve determination, Varuna was compared with a network of field reference stars in each image. The field stars were selected to be near Varuna in the sky and to have Sun-like or slightly redder colors. Where possible, we employed the same field reference stars each night, to minimize systematic photometric errors. This procedure effectively removes the influence of atmospheric extinction (which, at the high altitude of Mauna Kea, is already small, amounting to only about 0.08 mag per air mass in the R band). The latter part of the night of UT 2001

February 19 was slightly nonphotometric (deviations were roughly a few hundredths of a magnitude), but otherwise we benefited from clear skies. Effects of seeing variations between images were minimized by using multiaperture photometry. Small apertures (typical radii $\sim 1''$) were used to relate Varuna to the field star network in each field. Large apertures (typical radii $\sim 3''.0$) were used to relate the field stars to the Landolt standards. The median sky level was determined within a contiguous annulus having outer radius $5''$. At the time of the observations, Varuna moved westward at about $2''$ hr^{-1}. The image trailing due to the motion of Varuna was only $\sim 0''.1$ during a typical 200 s integration. This is small compared with our nominal $0''.7$ FWHM image quality, and therefore trailing losses are an unimportant source of error in our photometry.

A journal of observations, including the geometric circumstance, is given in Table 1. The R-band photometry is listed in Table 2. Periodicity in the photometry was obvious even in preliminary reductions of the first night's data conducted at the telescope, as may be seen in Figure 1.

3. RESULTS

The apparent magnitude varied in the approximate range 19.50–19.95, with a mean near 19.7. Periodicity in the R-band photometry was sought using (1) the PDM (phase dispersion minimization) method (Stellingwerf 1978) and (2) the related but different SLM (string length minimization) method (Dworetsky 1983). The PDM and SLM results were in all cases consistent; for brevity we here present only the results from PDM. Figure 2 shows the PDM theta parameter as a function of rotational frequency for the entire R-band photometry data set (the closer theta is to zero, the better the fit; see Stellingwerf 1978 for more information). Broad, deep minima occur near the light curve frequencies $P^{-1} = 7.57$ and 3.78 day^{-1}. The first corresponds to a single-peaked light curve with a period near $P = 3.17$ hr, close to the 3.17 hr period reported by Farnham (2001). The second minimum corresponds to the double-peaked light curve of 6.34 hr. The minima are flanked by aliases due to the 24 hr sampling periodicity that is imposed on the data by the day-night cycle (see the theta minima in Fig. 2, displaced from the primary by $\pm n$ day^{-1}, where $n = 1, 2, 3, \ldots$). The phased light curves produced using the 24 hr alias periods of the single-peaked light curve ($P^{-1} = 6.5$ day^{-1}, 8.6 day^{-1}) are unconvincing. When viewed at high resolution, the primary minimum of the theta plot for the single-peaked light curve is seen to be split by a finely spaced series of minima, as a result of the $\sim$65 day data gap between the 2001 February and April observations (Fig. 3). The light curves produced by phasing the data at each of the three lowest minima in Figure 3 (3.1656, 3.1721, and 3.1788 hr) appear comparably good to the eye. In this sense, the rotation period cannot be exactly determined from the present data, although we are confident that, if Varuna's light curve is single-peaked, the true period is given by one of the three minima in Figure 3. Subject to this caveat, we adopt $P = 3.1721 \pm 0.0001$ hr as the best fit to the single-peaked light curve period.

Is the light curve single- or double-peaked? Close inspection of the raw and phased data suggests that the light curve of Varuna has two maxima per rotation period. This is evident in Figure 4, where phased light curves show that the first and second light curve minima have slightly different shapes. Therefore, we adopt the double-peaked light curve ($P_{\rm rot} = 6.3442 \pm 0.0002$ hr) as the probable rotation period of Varuna (subject to the caveat that very nearby alias periods 6.3317 and 6.3574 hr are also plausible fits to the data, as discussed for the single-peaked aliases above). Our best estimate for the photometric range of the data is $\Delta m = 0.42 \pm 0.02$ mag.

We used the preliminary photometry to target color measurements near the extrema of the R-band brightness, in order to search for rotational color variations. Color measurements in B, V, and I filters were interleaved with R-band photometry so as to correct for photometric trends caused by the rotation. The color measurements are summarized in Table 3 and plotted versus rotation phase in Figure 5. There it may be seen that our data provide no evidence of rotational modulation of the color of the scattered radiation. Specifically, the $B-V$, $V-R$, and $R-I$ color indexes are constant with rotational phase at the level of accuracy of the measurements, as seen in Table 3. The mean colors found for Varuna, $B-V = 0.85 \pm 0.02$, $V-R = 0.64 \pm 0.01$, $R-I = 0.62 \pm 0.01$, and $B-I = 2.11 \pm 0.02$ (Table 3) are compatible with the mean colors of 12 other classical TNOs

TABLE 1
Journal of Observations for Varuna

UT Date[a] (2001)	JD[b] (2,450,000+)	Filters[c]	Seeing[d] (arcsec)	R[e] (AU)	Δ[f] (AU)	α[g] (deg)	t_L[h] (minutes)
Feb 17........	1,957.5	R	1.1	43.0539	42.4039	0.99	352.6621
Feb 18........	1,958.5	V, R	0.7	43.0540	42.4171	1.01	352.7725
Feb 19........	1,959.5	R, B, I	0.6	43.0542	42.4306	1.02	352.8845
Feb 20........	1,960.5	R	0.7	43.0543	42.4443	1.04	352.9981
Apr 22........	2,021.5	V, R	0.7	43.0632	43.4447	1.23	361.3187
Apr 24........	2,023.5	R	0.7	43.0635	43.4764	1.21	361.5823
Apr 25........	2,024.5	R	0.7	43.0636	43.4921	1.20	361.7126

[a] Universal Time date of the observation.
[b] Corresponding Julian Date at 0 hr UT.
[c] Filters based on the Johnson-Kron-Cousins system.
[d] Image FWHM.
[e] Heliocentric distance.
[f] Geocentric distance.
[g] Phase angle.
[h] Light travel time.

TABLE 2

R-Band Photometry of Varuna

Image Number	UT Date (2001)[a]	JD_c[b] (2,450,000 +)	m_R[c]	$m_R(1, 1, 0)$[d]
2019	Feb 17.2447	1,957.49983	19.913	3.450
2020	Feb 17.2484	1,957.50464	19.914	3.451
2021	Feb 17.2547	1,957.51099	19.898	3.435
2022	Feb 17.2592	1,957.51550	19.880	3.417
2023	Feb 17.2627	1,957.51904	19.860	3.397
2024	Feb 17.2662	1,957.52246	19.785	3.322
2025	Feb 17.2698	1,957.52600	19.776	3.313
2026	Feb 17.2733	1,957.52954	19.732	3.269
2027	Feb 17.2769	1,957.53320	19.689	3.226
2028	Feb 17.2805	1,957.53674	19.670	3.207
2029	Feb 17.2840	1,957.54028	19.659	3.196
2030	Feb 17.2876	1,957.54382	19.598	3.135
2032	Feb 17.2998	1,957.55603	19.562	3.099
2033	Feb 17.3033	1,957.55957	19.581	3.118
2034	Feb 17.3068	1,957.56311	19.553	3.090
2035	Feb 17.3105	1,957.56677	19.581	3.118
2036	Feb 17.3140	1,957.57019	19.599	3.136
2037	Feb 17.3175	1,957.57373	19.617	3.154
2038	Feb 17.3211	1,957.57739	19.658	3.195
2039	Feb 17.3247	1,957.58093	19.673	3.210
2040	Feb 17.3282	1,957.58447	19.705	3.242
2041	Feb 17.3339	1,957.59009	19.745	3.282
2042	Feb 17.3374	1,957.59363	19.820	3.357
2043	Feb 17.3410	1,957.59717	19.834	3.371
2044	Feb 17.3445	1,957.60083	19.878	3.415
2045	Feb 17.3481	1,957.60437	19.911	3.448
2046	Feb 17.3517	1,957.60791	19.909	3.446
2047	Feb 17.3552	1,957.61145	19.942	3.479
2048	Feb 17.3588	1,957.61499	19.922	3.459
2049	Feb 17.3624	1,957.61865	19.942	3.479
2051	Feb 17.3736	1,957.62976	19.888	3.425
2052	Feb 17.3771	1,957.63342	19.888	3.425
2053	Feb 17.3807	1,957.63696	19.872	3.409
2054	Feb 17.3842	1,957.64050	19.829	3.366
2055	Feb 17.3878	1,957.64404	19.824	3.361
2057	Feb 17.3978	1,957.65405	19.731	3.268
2058	Feb 17.4014	1,957.65759	19.679	3.217
2059	Feb 17.4050	1,957.66125	19.654	3.191
2060	Feb 17.4085	1,957.66479	19.614	3.151
2061	Feb 17.4121	1,957.66833	19.626	3.163
2062	Feb 17.4157	1,957.67200	19.615	3.152
2063	Feb 17.4193	1,957.67554	19.540	3.077
2064	Feb 17.4228	1,957.67908	19.610	3.147
2065	Feb 17.4264	1,957.68262	19.505	3.042
2066	Feb 17.4300	1,957.68628	19.506	3.043
2067	Feb 17.4337	1,957.68994	19.567	3.104
2068	Feb 17.4373	1,957.69360	19.569	3.106
2069	Feb 17.4409	1,957.69714	19.557	3.094
2070	Feb 17.4445	1,957.70081	19.583	3.120
2072	Feb 17.4543	1,957.71057	19.643	3.180
2073	Feb 17.4579	1,957.71411	19.687	3.224
2074	Feb 17.4614	1,957.71765	19.708	3.245
2075	Feb 17.4650	1,957.72131	19.753	3.290
3025	Feb 18.2337	1,958.48987	19.536	3.071
3026	Feb 18.2396	1,958.49585	19.603	3.138
3027	Feb 18.2432	1,958.49939	19.613	3.148
3028	Feb 18.2468	1,958.50305	19.634	3.169
3029	Feb 18.2503	1,958.50647	19.661	3.196
3031	Feb 18.2575	1,958.51367	19.758	3.293
3033	Feb 18.2646	1,958.52075	19.836	3.371
3035	Feb 18.2718	1,958.52795	19.909	3.444
3037	Feb 18.2789	1,958.53503	19.939	3.474
3039	Feb 18.2861	1,958.54224	19.969	3.504
3049	Feb 18.3223	1,958.57849	19.799	3.334

TABLE 2—*Continued*

Image Number	UT Date (2001)[a]	JD_c[b] (2,450,000+)	m_R[c]	$m_R(1, 1, 0)$[d]
3051	Feb 18.3295	1,958.58569	19.731	3.265
3053	Feb 18.3366	1,958.59277	19.673	3.208
3055	Feb 18.3439	1,958.60010	19.632	3.167
3057	Feb 18.3510	1,958.60718	19.581	3.116
3059	Feb 18.3582	1,958.61438	19.573	3.108
3074	Feb 18.4277	1,958.68384	19.931	3.466
3075	Feb 18.4314	1,958.68762	19.955	3.490
3076	Feb 18.4349	1,958.69104	19.864	3.399
3077	Feb 18.4385	1,958.69470	19.852	3.387
3078	Feb 18.4421	1,958.69824	19.833	3.368
3079	Feb 18.4457	1,958.70178	19.801	3.336
3080	Feb 18.4492	1,958.70532	19.766	3.301
4025	Feb 19.2381	1,959.49414	19.835	3.367
4026	Feb 19.2417	1,959.49780	19.798	3.330
4027	Feb 19.2452	1,959.50134	19.771	3.303
4030	Feb 19.2586	1,959.51465	19.628	3.160
4033	Feb 19.2753	1,959.53137	19.537	3.069
4036	Feb 19.2883	1,959.54443	19.544	3.076
4039	Feb 19.3016	1,959.55774	19.625	3.157
4044	Feb 19.3273	1,959.58350	19.891	3.423
4047	Feb 19.3405	1,959.59656	19.928	3.460
4050	Feb 19.3536	1,959.60974	19.951	3.483
4062	Feb 19.4036	1,959.65967	19.592	3.124
4065	Feb 19.4167	1,959.67285	19.565	3.097
5024	Feb 20.2402	1,960.49622	19.754	3.283
5025	Feb 20.2437	1,960.49976	19.792	3.321
5026	Feb 20.2473	1,960.50330	19.841	3.370
5030	Feb 20.2722	1,960.52820	19.961	3.490
5031	Feb 20.2758	1,960.53186	19.965	3.494
5032	Feb 20.2794	1,960.53540	19.933	3.462
5033	Feb 20.2830	1,960.53906	19.915	3.444
5034	Feb 20.2866	1,960.54260	19.893	3.422
5035	Feb 20.2902	1,960.54614	19.849	3.378
5036	Feb 20.2937	1,960.54980	19.855	3.384
5041	Feb 20.3273	1,960.58337	19.574	3.103
5042	Feb 20.3312	1,960.58716	19.565	3.094
5044	Feb 20.3430	1,960.59900	19.548	3.077
5045	Feb 20.3468	1,960.60278	19.569	3.098
5046	Feb 20.3506	1,960.60669	19.583	3.112
5047	Feb 20.3545	1,960.61047	19.566	3.095
3022	Apr 22.2417	2,021.49219	19.776	3.224
3023	Apr 22.2458	2,021.49634	19.746	3.194
3036	Apr 22.2861	2,021.53699	19.655	3.103
3038	Apr 22.2958	2,021.54663	19.745	3.193
5015	Apr 24.2523	2,023.50269	19.615	3.064
5016	Apr 24.2565	2,023.50696	19.616	3.065
5021	Apr 24.2853	2,023.53564	19.807	3.256
5022	Apr 24.2896	2,023.53992	19.857	3.306
6018	Apr 25.2382	2,024.48853	20.005	3.455
6019	Apr 25.2425	2,024.49280	20.037	3.487
6026	Apr 25.2863	2,024.53662	19.718	3.168
6027	Apr 25.2906	2,024.54089	19.695	3.145

[a] Decimal Universal Date at the start of the integration.
[b] Julian Date corrected to the midpoint of each integration and for light travel time.
[c] Apparent red magnitude; uncertainties are ± 0.02.
[d] Absolute magnitude found using $m_R(1, 1, 0) = m_R - 5\log(R\Delta) - \beta_{\rm opp}\alpha$ where $\beta_{\rm opp} = 0.156$ mag deg^{-1} (see Sheppard & Jewitt 2002).

measured independently (Jewitt & Luu 2001: $B-V = 1.00 \pm 0.04$, $V-R = 0.61 \pm 0.03$, $R-I = 0.60 \pm 0.04$, and $B-I = 2.22 \pm 0.10$). Although larger than most, Varuna is not colorimetrically distinguished from the other TNOs.

4. INTERPRETATION

The rotational light curve of a solar system body results from the combined effects of aspherical body shape and azimuthal albedo variations. Double-peaked light curves are

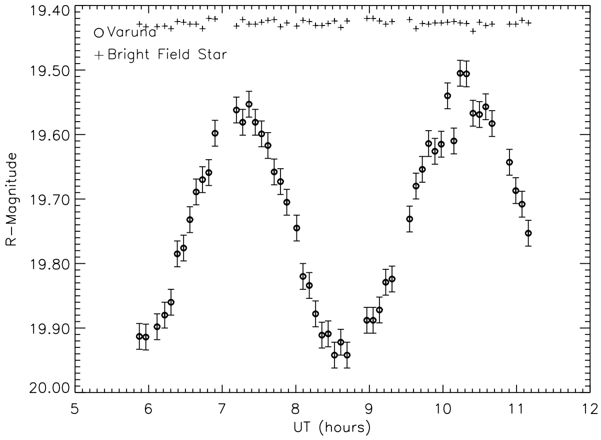

FIG. 1.—Sample rotational light curve data for Varuna from UT 2001 February 17. Error bars of ± 0.02 mag plotted for reference.

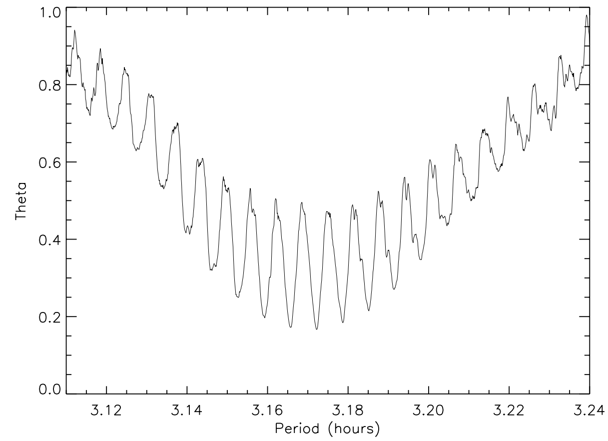

FIG. 3.—Same as Fig. 2, but with period as the *x*-axis and at higher resolution on the single-peaked best fit, to show the aliases caused by the ~ 60 day gap between the February and April observations. The three lower peaks are all reasonable fits to the data, with the middle peak at 3.1721 hr being the best fit for the single-peaked light curve.

the expected signature of an elongated body in rotation about its minor axis. However, this interpretation is not unique: an appropriate arrangement of albedo markings can reproduce any light curve (Russell 1906). The large size of Varuna suggests that any elongation of the body is probably caused by a large specific angular momentum and the resulting rotational deformation. Here we consider the two limiting cases in which (1) the light curve is produced entirely by albedo variations across the surface of Varuna and (2) the light curve is produced by rotational modulation of the geometric cross section of Varuna due to aspherical shape. The real situation of Varuna will naturally lie somewhere between these two extremes.

4.1. *Albedo Models*

A complex distribution of albedo markings could produce the observed light curve. If so, the $\Delta m_R = 0.42 \pm 0.02$ mag photometric range would imply an albedo contrast $10^{0.4\Delta m_R} \approx 3:2$ or greater (depending on the projection of the rotation vector into the line of sight). Some spherical outer solar system bodies show large albedo contrasts, notably Iapetus (Millis 1977) and Pluto (Buie, Tholen, & Wasserman 1997). On Iapetus, the albedo contrast is associated with a color variation, the dark material being redder than the bright material (Table 4). Rotational color variations on Varuna as large as those on Iapetus would be apparent in our data if they were present. Pluto's hemispherical albedo contrast is matched by a corresponding color variation that is barely measurable even in this bright object (Table 4). Large color differences exist between local surface units on Pluto ($0.77 \leq B-V \leq 0.98$; Young, Binzel, & Crane 2001), but hemispherically averaged color variations occur only at the 0.01 mag level and are so small that they would not be detected in the present work (Table 4). From the example set by Pluto, we conclude that the absence of color variations on Varuna larger than a few times 0.01 mag places no useful constraint on the albedo modulation hypothesis.

If Varuna is spherical and rotating at period P, we can obtain a lower limit to the density by requiring that the body not be in a state of internal tension. Simple force balance

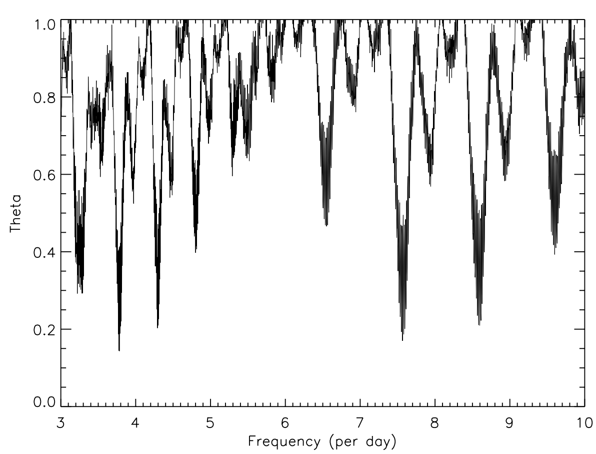

FIG. 2.—Phase dispersion minimization (PDM) plot computed from the entire *R*-band data set of Varuna (February and April observations). The best fit is the frequency near 3.78 cycles day^{-1} (double-peaked period of 6.34 hr). The other large peaks flanking the 3.78 frequency are the 24 hr sampling aliases. The single-peaked period is at 7.57 cycles day^{-1} (period of 3.17 hr), with associated flanking 24 hr alias periods.

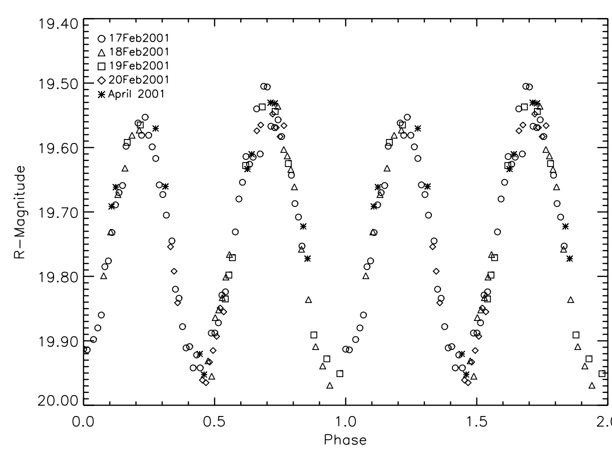

FIG. 4.—*R*-band photometry of Varuna, phased according to the double-peaked rotation period $P_{\rm rot} = 6.3442$ hr. The April data have been brightened by 0.09 mag to correct for the dimming effects of a higher phase angle (see Sheppard & Jewitt 2002) and greater distance of Varuna compared with the February observations.

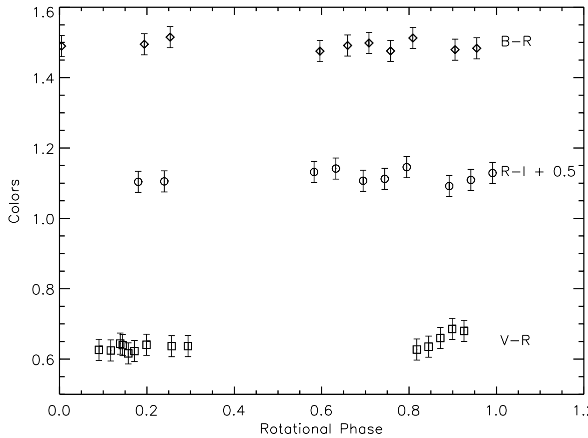

FIG. 5.—$B-R$, $R-I$, and $V-R$ colors of Varuna, showing no significant variation over its rotation. The $R-I$ colors have been shifted up by 0.5 mag for clarity in distinguishing them from the $V-R$ colors.

then gives

$$\rho = 3\pi/GP^2, \tag{1}$$

where $G = 6.67 \times 10^{-11}$ (N kg^{-2} m^2) is the gravitational constant and $P(s)$ is the rotation period. With $P = 3.17$ hr, equation (1) yields a lower limit to the density as $\rho = 1090$ kg m^{-3}. The hydrostatic pressure at the center of a 450 km radius object with this density is $\sim 6 \times 10^7$ N m^{-2}. A body as large as Varuna will almost certainly not possess the strength needed to maintain spherical shape when rotating with a 3 hr period (note that the rotations of the comparison objects Iapetus and Pluto are tidally locked, with periods 79 and 6.4 *days*, respectively, so that rotational deformation is small). Therefore, we believe that the spherical albedo model of Varuna is physically implausible. Instead, we next discuss models in which the shape, not the albedo, is primarily responsible for the observed light curve variations.

TABLE 3
COLOR MEASUREMENTS OF VARUNA

UT Date (2001)	Image Number	JD_c[a] (2,450,000+)	Phase[b]	R[c]	$B-R$	$V-R$	$R-I$
Feb 18	3030	1,958.5101	0.818	19.71	...	0.63	...
Feb 18	3032	1,958.5172	0.845	19.78	...	0.64	...
Feb 18	3034	1,958.5244	0.872	19.85	...	0.66	...
Feb 18	3036	1,958.5316	0.899	19.91	...	0.69	...
Feb 18	3038	1,958.5387	0.926	19.94	...	0.68	...
Feb 18	3050	1,958.5786	0.090	19.77	...	0.63	...
Feb 18	3052	1,958.5894	0.117	19.71	...	0.62	...
Feb 18	3054	1,958.5966	0.144	19.64	...	0.64	...
Feb 18	3056	1,958.6038	0.171	19.59	...	0.62	...
Feb 18	3058	1,958.6108	0.199	19.56	...	0.64	...
Feb 19	4028	1,959.5052	0.583	19.72	...	...	0.63
Feb 19	4029	1,959.5099	0.596	19.69	1.48	...	...
Feb 19	4031	1,959.5183	0.632	19.61	...	...	0.64
Feb 19	4032	1,959.5266	0.659	19.57	1.49	...	...
Feb 19	4034	1,959.5349	0.695	19.54	...	...	0.61
Feb 19	4035	1,959.5396	0.708	19.54	1.50	...	...
Feb 19	4037	1,959.5480	0.744	19.56	...	...	0.61
Feb 19	4038	1,959.5530	0.758	19.58	1.48	...	...
Feb 19	4040	1,959.5612	0.795	19.65	...	...	0.65
Feb 19	4041	1,959.5663	0.809	19.69	1.51	...	...
Feb 19	4045	1,959.5870	0.892	19.89	...	...	0.59
Feb 19	4046	1,959.5917	0.905	19.92	1.48	...	...
Feb 19	4048	1,959.6001	0.941	19.95	...	...	0.61
Feb 19	4049	1,959.6047	0.955	19.96	1.48	...	...
Feb 19	4051	1,959.6132	0.991	19.95	...	...	0.63
Feb 19	4052	1,959.6179	0.005	19.94	1.49	...	...
Feb 19	4063	1,959.6632	0.180	19.58	...	...	0.60
Feb 19	4064	1,959.6680	0.194	19.57	1.49	...	...
Feb 19	4066	1,959.6777	0.240	19.57	...	...	0.61
Feb 19	4067	1,959.6812	0.253	19.58	1.52	...	...
Apr 22	3024	2,021.5009	0.139	19.66	...	0.64	...
Apr 22	3025	2,021.5057	0.157	19.62	...	0.62	...
Apr 22	3035	2,021.5303	0.257	19.58	...	0.64	...
Apr 22	3037	2,021.5420	0.294	19.66	...	0.64	...
Mean					1.49 ± 0.01	0.64 ± 0.01	0.62 ± 0.01

[a] Julian day at midexposure, corrected for light travel time.
[b] Rotational phase of Varuna light curve with period 6.34 hr. The phase corresponds to Fig. 4, where 0.45 and 0.95 are minimum light ($\sim$19.9) and 0.20 and 0.70 are maximum light ($\sim$19.5) of the double-peaked light curve.
[c] R magnitude interpolated to the time of the corresponding BVI data.

TABLE 4
Comparison of Rotational Color Variations

Object	Δm (mag)	$\Delta m(B-V)$ (mag)	Reference
Varuna........	0.42 ± 0.02	<0.02	This work
Iapetus........	~2	0.07–0.10	Millis 1977
Pluto...........	0.35	0.01	Buie et al. 1997

4.2. *Shape Models*

A more likely model is one in which Varuna is rotationally deformed by the centripetal forces associated with its rapid rotation. As in the asteroid belt, large impacts that do not completely destroy a body may disrupt it into a self-gravitationally bound, strengthless "rubble pile" (Farinella et al. 1981). Rubble pile bodies will reassemble after impact into a shape determined by their angular momentum, H, and density, ρ. Following the convention of Chandrasekhar (1987), we write the angular momentum in units of $(GM^3a')^{1/2}$, where M (kilograms) is the body mass and a' (meters) is the radius of the equal-volume sphere. At $H = 0$, the equilibrium shape is the sphere. As H increases, a perfectly strengthless fluid deforms first into an oblate (so-called MacLaurin) spheroid in rotation about its minor axis (Chandrasekhar 1987). The MacLaurin spheroids become progressively more flattened up to the critical value $H = 0.304$, above which the body becomes triaxial (a Jacobi spheroid). At $H \geq 0.390$, the Jacobi spheroids are rotationally unstable, and the object splits into a binary. This rotational deformation sequence is highly idealized when applied to solid bodies, of course, because even a rubble pile will not respond to rotational stresses in the same way as a perfectly strengthless fluid. A fractured body will have a "grainy" structure, perhaps with large, coherent internal blocks that will retain expression in the final body shape. Nevertheless, the MacLaurin-Jacobi spheroids represent a limiting case with which the asteroids and TNOs may usefully be compared. Evidence of the existence of rubble piles among the main-belt asteroids is limited and indirect but nevertheless suggestive. For example, small asteroids ($D \leq 100$ km) have a distribution of body shapes that is consistent with those of fragments from hypervelocity-impact experiments in the laboratory (Catullo et al. 1984). On the other hand, larger asteroids are deficient in highly elongated bodies relative to the fragment shape distribution, perhaps because their shapes have relaxed toward rotational equilibrium (Farinella et al. 1981). As we note below, a few well-measured asteroids have densities less than the density of solid rock, suggesting a porous internal structure that could be produced by reaccumulation of large blocks in a rubble pile (Yeomans et al. 1997). TNOs larger than about 100 km in diameter are massive enough to survive collisional disruption over the age of the solar system, but may nevertheless have been internally fractured into rubble piles (Farinella & Davis 1996).

Since an oblate spheroid in principal axis rotation about its axis of maximum moment of inertia offers no rotational modulation of the cross section, we conclude that the MacLaurin spheroids cannot explain the light curve of Varuna and that $H > 0.304$ for this object. However, the triaxial Jacobi spheroids with $0.304 \leq H \leq 0.390$ present plausible solutions for the shape of Varuna. For the Jacobi spheroids, knowledge of the rotation period and the shape

TABLE 5
Shape Models and Density For Varuna

Model	Shape	Axis Ratios[a]	Density ($\mathrm{kg\ m^{-3}}$)
Albedo Spots	Sphere	1 : 1 : 1	≥1090
Jacobi	Ellipsoid	≥1.5 : 1.0 : 0.7	≥1050
Binary.................	Contact Spheres	≥1.4 : 1	≥996
	Roche ellipsoids	1.06 : 1, 1.67 : 1	3600

[a] For the binary models, the listed "axis ratio" is the ratio of the diameters of the separate components.

(from Δm) provides a unique measure of the density. With $P = 6.34$ hr and axis ratio $10^{0.4\Delta m} \approx 3:2$, we obtain $\rho = 1050\ \mathrm{kg\ m^{-3}}$ from the tables of Chandrasekhar (1987; also, see Table 5). Since the axis ratio can only be a lower limit (because of projection), the derived density is also a lower limit. This value is close to the density estimated from the spherical albedo model above, but has the advantage that it is derived from a physically more plausible model. A Jacobi ellipsoid's three axes ($a > b > c$) depend strongly on each other. Using the axis ratio for a and b above, we find the ratio for all three to be 3 : 2 : 1.4 (Chandrasekhar 1987). Here 1.4 refers to the rotation axis (c), which cannot be observed directly through the light curve if the object is in principal axis rotation.

4.3. *Binary*

We also consider the possibility that Varuna is a binary, in which case the light curve would result from occultation of one component by the other. The short period and light curve shape of Varuna require that the binary components must be close, or even in contact, leading to mutual gravitational deformation of the components. We will consider these effects momentarily. However, it is physically illuminating to first discuss the limiting case in which the binary components are in contact but retain a spherical shape. Suppose that the primary and secondary components have radii a_p and a_s, respectively. The barycenter of the contact binary will be separated from the center of the secondary by a distance

$$l = (a_p + a_s)\left(\frac{m_p}{m_p + m_s}\right), \tag{2}$$

where m_p and m_s are the masses of the primary and secondary, respectively. Force balance then gives a relation between the angular frequency, density, and mass ratio, namely $l\omega^2 = Gm_p/(a_p + a_s)^2$. Assuming that both components have density ρ ($\mathrm{kg\ m^{-3}}$), we obtain

$$\rho = \frac{3\pi}{GP^2}\frac{\left[1 + (a_s/a_p)\right]^3}{1 + (a_s/a_p)^3}. \tag{3}$$

The ratio a_s/a_p can be estimated from the photometric range of the light curve. Specifically, the range in magnitudes is given by

$$\Delta m = 2.5\ \log\left(\frac{\mathrm{a_s^2 + a_p^2}}{\mathrm{a_p^2}}\right), \tag{4}$$

which can be rearranged to give

$$\frac{a_s}{a_p} = (10^{0.4\Delta m} - 1)^{1/2}. \tag{5}$$

From equation (5), the Varuna light curve range ($\Delta m = 0.42$ mag) suggests an axis ratio $a_s/a_p = 0.69$, corresponding to mass ratio $m_s/m_p = (a_s/a_p)^3 = 0.32$. Equations (3) and (5) together give the density in terms of the two observable quantities P and Δm:

$$\rho = \frac{3\pi}{GP^2} \frac{\left[1 + (10^{0.4\Delta m} - 1)^{1/2}\right]^3}{1 + (10^{0.4\Delta m} - 1)^{3/2}} . \quad (6)$$

Substitution of $P = 6.3$ hr and $\Delta m = 0.42$ mag into equation (6) yields $\rho = 996$ kg m^{-3}. This is a lower limit to the density since, because of projection effects, the observations provide only a lower limit to Δm. However, given the crudeness of this model, it is interesting that we obtain essentially the same density as from the Jacobi spheroid approximation. We conclude that binary models with the observed period and physically plausible densities can account for the Varuna light curve. There remains, however, no specific evidence that Varuna is a binary object.

Finally, Leone et al. (1984) present calculations that partly account for the mutual deformation of the components in a close binary. The solutions are nonunique, since different combinations of m_s/m_p and density lead to the same P, Δm pair. Here, we simply refer to their Table 1 and note a plausible solution near $\rho \approx 3600$ kg m^{-3} and $m_s/m_p \approx 0.2$. This bulk density is much higher than is required than in our simple, spherical, contact binary model, since the components are more widely separated (the Roche radius is about twice the component radius) and therefore orbit more slowly for a given mass. For several reasons, we believe that the Roche model and the Leone et al. calculations are not well suited to the case of Varuna. In particular, the wide separation reduces the probability that the system would be aligned so as to produce mutual eclipses. Furthermore, the nearly sinusoidal light curve shape is not easily produced by a widely separated pair, in which we would expect the eclipses and occultations to occupy a smaller fraction of rotational phase space. Varuna's light curve does not show the notched appearance characteristic of eclipsing binary stars.

5. DISCUSSION

5.1. *The Density of Varuna*

The bulk density derived in § 4 is only slightly higher than the density of water ice. Strictly speaking, the derived density is a lower limit, because of the effects of projection into the plane of the sky. However, it is unlikely that the density is much (factor of 2) higher than 1000 kg m^{-3}, if our equilibrium rotator model is correct. The simplest interpretation, namely that the rock content of Varuna is small or negligible, is difficult to accept on physical grounds: accretion of planetary solids in a dusty circumsolar disk provides no obvious fractionation mechanism to lead to the formation of a pure ice ball. Here, we explore the possibility that Varuna's low density is caused by an internal structure that is at least partly porous.

We represent Varuna as a composite of volatile matter (ice), refractory matter (rock), and void space. The mean density of this composite is

$$\overline{\rho} = \rho_i f_i + \rho_r f_r , \quad (7)$$

where ρ_i and ρ_r are the densities of ice and rock, and f_i and f_r are the fractional volumes occupied by ice and rock, respectively. We require

$$f_i + f_r + f_v \equiv 1 , \quad (8)$$

where f_v is the fractional void space, also known as porosity. The fraction of the total mass carried by refractories is

$$\psi = \frac{\rho_r f_r}{\rho_r f_r + \rho_i f_i} . \quad (9)$$

Equations (7)–(9) combine to yield

$$f_v = 1 - \frac{\overline{\rho}}{\rho_i}\left[1 + \psi\left(\frac{\rho_i}{\rho_r} - 1\right)\right] . \quad (10)$$

The hydrostatic pressure at the core of Varuna is about 6×10^7 N m^{-2}, while the mass-weighted internal temperatures are likely to average $\sim$100 K ($\sim$50 K at the surface, slowly rising toward the core as a result of internal radioactive decay heating). Under these conditions the ice-I polymorph of water, for which $\rho_i = 940$ kg m^{-3} (Lupo & Lewis 1979), is the stable phase. The density of the refractory matter, ρ_r, is less certain, and we compute models using two representative values. First, we take $\rho_r = 3000$ kg m^{-3} as representative of the densities of a number of plausible silicates, notably forsterite (Mg_2SiO_4), which has been spectroscopically detected in comets. Second, we take $\rho_r = 2000$ kg m^{-3} to represent the less dense CHON-type hydrocarbon materials that are also found in comets.

The resulting values of the porosity are plotted against the rock fraction in Figure 6, where we have adopted $\overline{\rho} = 1000$ kg m^{-3} (*solid lines*) from the light curve models. To show the sensitivity to the mean density, we also plot in Figure 6 the porosities derived if $\overline{\rho} = 1200$ kg m^{-3} (*dashed lines*).

Figure 6 shows that nonporous ($f_v = 0$) models restrict the rock fraction ψ to between $\sim$0.1 (for $\overline{\rho} = 1000$ kg m^{-3}) and $\sim$0.35 (for $\overline{\rho} = 1200$ kg m^{-3}). Larger rock fractions require nonzero porosity; cosmochemically plausible $\psi = 0.5$ implies $0.05 \leq f_v \leq 0.30$ for the parameters considered here. The few measured nuclei of comets have densities in the range 500–1000 kg m^{-3} (Sagdeev, Elyasberg, & Moroz 1988; Rickman 1989; Asphaug & Benz 1996) and rock fractions $\psi \geq 0.5$ (corresponding to rock : ice mass ratios $\geq$1; Lisse et al. 1998; Jewitt & Matthews 1999). Given that the Jupiter-family comets are collisionally produced fragments of the trans-Neptunian objects (Farinella & Davis 1996), large ψ may well be representative of Varuna and related objects.

Are porosities up to several tens of percent physically plausible in a body of Varuna's size? We argue first by analogy. Materials on planetary surfaces are commonly porous. Carbonate ($CaCO_3$) Waikiki beach sand, for instance, has porosity $f_v \sim 0.4$, while the basaltic lunar regolith has $0.4 \leq f_v \leq 0.7$ (Carrier, Mitchell, & Mahmood 1974). The mechanical compression of carbonate and quartz sands (SiO_2) has been studied experimentally to pressures rivalling that in Varuna's core (Chuhan, Kjeldstad, & Bjørlykke 2002). Sand samples having porosity $f_v = 0.4$–0.5 at atmospheric pressure compress only to $f_v \sim 0.2$–0.3 at 5×10^7 N m^{-2}. At pressures $\leq(2$–$6) \times 10^6$ N m^{-2}, the densification occurs by rearrangement of the irregular silicate grains while at higher pressures the densification occurs by grain crushing and the filling in of void space. Crushing is particu-

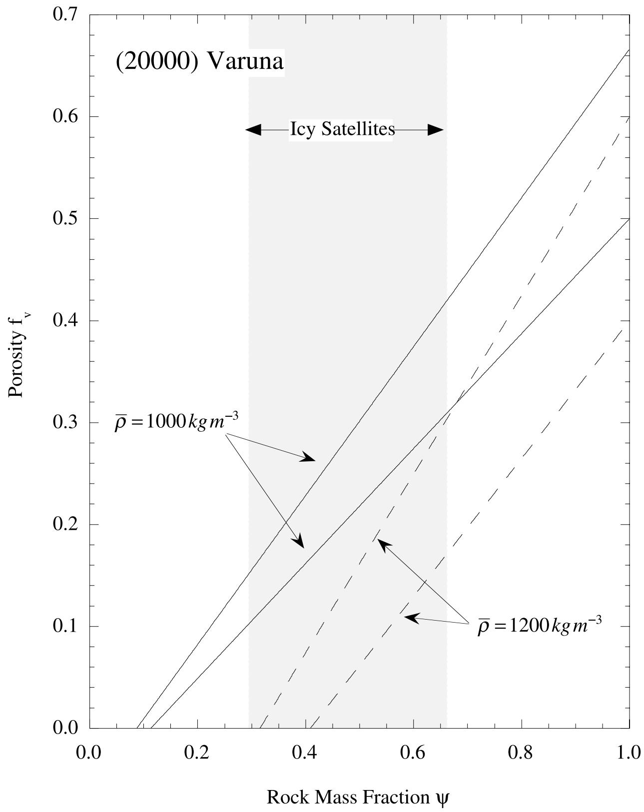

FIG. 6.—Porosity, f_v, vs. rock fraction, ψ, from eq. (10). Models for $\overline{\rho} = 1000$ kg m^{-3} and $\overline{\rho} = 1200$ kg m^{-3} are indicated. The upper (lower) line for each density refers to an assumed rock density $\rho_r = 3000$ (2000) kg m^{-3}. The range of rock fractions inferred for the icy satellites of Saturn and Uranus by Kossacki & Leliwa-Kopystyński (1993) is shown for comparison.

larly important in large-grain sands, where the number of grain-grain contacts is small and the contact pressures are high. In any event, this direct experimental evidence shows that aggregates of silicate (and carbonate) grains can remain substantially porous throughout the range of pressures prevailing inside Varuna. The physical reason is the large compressive strength of the grain materials.

At low temperatures, water ice also possesses a large compressive strength (1.2×10^8 N m^{-2} at 158 K, rising to 1.7×10^8 N m^{-2} at 77 K; Durham, Heard, & Kirby 1983), giving a response to hydrostatic loading qualitatively similar to that of sand. However, the experimental situation for ice-grain aggregates is less clear, mainly because most experiments have been performed at temperatures and strain rates higher than are relevant to outer solar system bodies. The most relevant experiments of which we are aware were conducted at 213 K over the (0.8–8.2) $\times 10^8$ N m^{-2} pressure range (Leliwa-Kopystyński et al. 1994). They show that substantial porosity can exist in ice–rock grain mixtures at all pressure levels found inside Varuna. We conclude that porosity is a potentially important factor in determining the bulk constitutions of the TNOs.

Several of the outer-planet satellites are similar to Varuna in both size and density. For example, Saturnian satellite SIII Tethys has density $\overline{\rho} = 1210 \pm 160$ kg m^{-3} and is 524 ± 5 km in radius (Smith et al. 1982). The Uranian satellite UII Umbriel has density 1440 ± 280 kg m^{-3} and radius 595 ± 10 km (Smith et al. 1986). Even the much larger and, presumably, self-compressed object Iapetus (radius 730 ± 10 km) has a low density, only 1160 ± 90 kg m^{-3} (Smith et al. 1982). Internal porosity (due to the granular structure of the constituent materials) may account for the low densities of these satellites, while simultaneously allowing rock fractions $0.28 \leq \psi \leq 0.66$ (Kossacki & Leliwa-Kopystyński 1993). Within the uncertainties, these bodies all have densities consistent with that derived here for Varuna. Unlike Varuna, they are nearly spherical in shape, but this is because the satellites are tidally locked, with rotation periods measured in days, not hours, and the centripetal accelerations are consequently very small. If rotating with Varuna's angular momentum, they would adopt elongated body shapes and display large rotational light curves.

The larger object Pluto has $\rho \approx 2000$ kg m^{-3} (Tholen & Buie 1997); the corresponding rock fraction from equation (10) (assuming $f_v = 0$ and considering higher pressure ice phases) is $\psi \sim 0.7$. Core hydrostatic pressure (which scales as $\rho^2 r^2$) is higher in Pluto than in Varuna by a factor of $\sim$25. For this reason, it is natural to expect that the influence of porosity on Pluto's bulk density should be greatly reduced relative to the Varuna case.

A different source of porosity is suggested by the 50 km diameter and (presumably) rocky main-belt asteroid 253 Mathilde, which is of surprisingly low density (1300 ± 200 kg m^{-3}; Yeomans et al. 1997). This low density may reflect macroscopic porosity ($\sim$50%) resulting from the loose reaccumulation of a fractured body into a rubble pile structure. In Varuna, microscopic and macroscopic porosity may coexist, the former from the slow accretion of grains at low temperatures and the latter from an energetic, terminal collision phase.

Varuna is one of the largest known trans-Neptunian objects, with a diameter $D = 900^{+125}_{-145}$ km (1 σ error bars; Jewitt et al. 2001). Even the 3 σ lower limit to the diameter, 465 km, leaves this an object of imposing dimensions. But Varuna is not entirely alone in its combination of large size, short period, and aspherical shape: there are a few large asteroids that have both large photometric ranges and short periods. Notable examples include 15 Eunomia (diameter 256 km, period 6.08 hr, photometric range 0.56 mag), 87 Sylvia (270 km, 5.18 hr, 0.62 mag), and 107 Camilla (222 km, 4.84 hr, 0.52 mag). Like Varuna, these may be bodies of low strength that are rotationally deformed because of a large amount of angular momentum delivered by collisions (Farinella et al. 1981). Collectively, these observations show that the low density of Varuna, as deduced from its light curve, is unremarkable when viewed in the context of other solar system objects.

5.2. *High Specific Angular Momentum in the Trans-Neptunian Belt*

The discussion in § 4 shows that Varuna must possess a high specific angular momentum, $0.304 \leq H \leq 0.390$, close to the value needed to cause rotational breakup. This immediately suggests a parallel with the four known trans-Neptunian binaries, Pluto-Charon (Tholen & Buie 1997), 1998 WW31 (Veillet 2001), 2001 QT297 (Elliot et al. 2001), and 2001 QW322 (Kavelaars et al. 2001), because these systems also possess high specific angular momenta. Of these four, Pluto-Charon is by far the best characterized (neither the sizes/masses nor the eccentricities of the other binary systems are yet known, preventing the determination of their specific angular momenta at a diagnostically useful level). In the Pluto-Charon system the angular momentum is primarily contained within the orbital motion of the components (i.e., the spin angular momentum is small). If the mass and angular momentum of Pluto and Charon were to be combined into a single body, that object would have $H \approx 0.45$ (McKinnon 1989) and would be unstable to rotational breakup. This fact suggests that Pluto and Charon were formed by a glancing impact between precursor objects (McKinnon 1989; Dobrovolskis, Peale, & Harris 1997). It is not yet clear that the other (much less massive) TNO binaries formed in a similar way, but their high specific angular momenta nevertheless suggest that collisions played an important role. We believe that Varuna is an intermediate case, in which a collision between massive precursors produced a spin rapid enough to cause global deformation but not sufficient to cause rotational breakup.

The current collision rate among trans-Neptunian objects is too low to substantially modify the spins of objects as large as Pluto and Varuna. Instead, their H must have been acquired through late-stage collisions at the end of the $\sim$100 Myr (Kenyon & Luu 1999) formation period. We use this to constrain the collisional environment in the young trans-Neptunian belt. Since the applicable parameters are not well known, an order of magnitude–type (particle-in-a-box) calculation is appropriate. Our objective is to estimate the density of objects in the trans-Neptunian belt needed to produce collisional breakup of a measurable fraction of the Varuna-sized objects within the 100 Myr formation period. Collisional breakup does not guarantee the formation of a binary and may not lead to a high specific angular momentum in the target object, but it is a necessary step toward these ends.

We first represent the TNO size distribution by a power law, in which the number of objects per unit volume with radii in the range a to $a + da$ is $n(a)\,da = \Gamma a^{-q}\,da$, where Γ and q are constants. The timescale for the collisional disruption of a nonrotating, spherical target TNO of radius a_T is given by

$$\tau^{-1} = \int_{a_C}^{\infty} 4\pi(a_T + a)^2 \Gamma a^{-q} \Delta V\, da. \tag{11}$$

Here, a_C is the critical radius of the smallest projectile capable of producing disruption and ΔV is the impact velocity. The constant Γ is obtained from the data by normalizing to the trans-Neptunian belt population, such that

$$\int_{a_{50}}^{\infty} \Gamma a^{-q}\, da = \frac{N_{50}}{W}, \tag{12}$$

where N_{50} is the number of TNOs larger than $a_{50} = 50$ km in radius, and W is the effective volume swept by the classical TNOs. We adopt $q = 4$, $\Delta V = 1.3$ km s^{-1}, and $N_{50} = 4 \times 10^4$ (Trujillo, Jewitt, & Luu 2001) and represent the classical belt as an annulus with inner and outer radii of 40 and 50 AU, respectively, and thickness of 10 AU, giving $W \approx 9.5 \times 10^{38}\ m^3$. Hence, $\Gamma = 1.6 \times 10^{-20}$ by equation (12).

For spherical target and projectile TNOs of equal density, the critical projectile radius for disruption is given by

$$\frac{a_C}{a_T} = \left(\frac{2\epsilon}{\Delta V^2}\right)^{1/3}, \tag{13}$$

where $\epsilon \approx 10^5$ J kg^{-1} is the specific energy for disruption (Love & Ahrens 1996).

Combining these relations and substituting, we obtain

$$\tau \approx 2.5\ \mathrm{Gyr}\left(\frac{a_T}{1\ \mathrm{km}}\right)\left(\frac{4 \times 10^4}{N_{50}}\right) \tag{14}$$

as our estimate of the collisional lifetime of a TNO of radius a_T in the present-day, low-density, trans-Neptunian belt. Varuna-scale objects ($a_T \sim 450$ km) have lifetimes to collisional disruption $\tau \sim 1 \times 10^{12}$ yr (eq. [14]), much longer than the 4.6×10^9 yr age of the solar system (Farinella & Davis 1996). Under these circumstances, large, collisionally produced binaries and objects of high specific angular momentum should not be common.

The frequencies of occurrence of both rotationally distorted and binary TNOs remain to be determined with accuracy. Objects 1998 SM165 and 2000 GN171 have independently been reported to show large rotational variations (Romanishin et. al 2001 and Sheppard 2001, respectively) and, from the available data, it seems likely that large-amplitude objects like Varuna are common, as are binary TNOs. We conservatively estimate that a fraction $f \geq 1\%$ of the TNOs are binaries and/or rotationally distorted objects of high intrinsic angular momentum. If the formation phase took $\tau_f \sim 10^8$ yr (Kenyon & Luu 1999), then the corresponding disruption timescale is of order $f^{-1}\tau_f \leq 10^{10}$ yr. With this timescale and $a_T = 450$ km (for Varuna), equation (14) yields $N_{50} \sim 5 \times 10^6$, about 100 times the current number of large TNOs. The current mass of the TNOs is about 0.1–0.2 $M_\oplus$ (Jewitt, Luu, & Trujillo 1998; Trujillo, Jewitt, & Luu 2001). Thus, from the high incidence of binaries and rotationally distorted objects, we infer an initial mass $M_i \geq$ 10–20 $M_\oplus$ (where 1 $M_\oplus = 6 \times 10^{24}$ Kg is the mass of the Earth) in the classical region of the trans-Neptunian belt. Numerical accretion calculations give the time for trans-Neptunian objects to grow to 1000 km scale as $\tau \sim$ 280 Myr (10 $M_\oplus/M_i$; Kenyon & Luu 1999). Substituting for M_i, we obtain $\tau \sim$ 140–280 Myr, comparable to the $\sim$100 Myr timescale estimated for the formation of Neptune.

Efficient growth of the TNOs required a small velocity dispersion. Growth models show that mutual scattering by ever larger bodies produced an increase in the velocity dispersion, ultimately resulting in collisional shattering of the smaller objects (Kenyon & Luu 1999). The broad inclination and eccentricity distributions of the current TNOs suggest that another process, perhaps the appearance of nearby Neptune or, conceivably, an external perturber (Ida, Larwood, & Burkert 2000), increased the velocity dispersion to values even higher than could be attained through mutual scattering. The collisional events leading to Varuna's rapid rotation and the breakup of TNOs probably occurred in this final stage.

Ongoing measurements of the light curves, spin states, and binarity of a statistical sample of TNOs will show the extent to which the shapes of these bodies are determined by their angular momenta (see Sheppard & Jewitt 2002). Detection of a large proportion of high-H objects would strengthen our conclusion that the past environment in the trans-Neptunian belt was one in which collisions between massive bodies were common. The role of porosity will be illuminated by future measurements of TNO densities, perhaps based on careful astrometric and physical studies of the growing sample of binary objects. We expect a trend toward higher densities at larger diameters, at least among those TNOs that have survived intact (although fractured) since the formation of the solar system. Smaller objects, particularly the 1–10 km scale bodies sampled locally in the Jupiter-family comets, may display a wide range of densities influenced both by the density (hence, size) of the target from which they were eroded and by densification during the collisional process.

6. SUMMARY

1. High-precision, time series photometry of trans-Neptunian object (20000) Varuna reveals a sustained, periodic modulation of the apparent brightness. In data from 2001 February and April, the best-fit rotation period is double-peaked, with a 6.3442 ± 0.0002 hr period. The photometric range is $\Delta m = 0.42 \pm 0.02$ mag. The $B-V$, $V-R$, and $R-I$ colors are completely typical of TNOs and show no variation with rotational phase, down to the level of a few percent.

2. We interpret Varuna as a centripetally distorted body, with an axis ratio $\geq 3:2$ and density $\rho \approx 1000$ kg m^{-3}. The specific angular momentum, $0.304 \leq H \leq 0.390$, is high (objects with $H > 0.390$ are rotationally unstable and break up).

3. The low bulk density of Varuna requires significant porosity (up to several tens of percent) if the rock mass fraction is cosmochemically typical ($\sim$0.5). In this respect, Varuna is similar to the icy satellites of Saturn and Uranus, many of which show bulk densities near that of water ice. Porosity could occur on a microscopic level, because of granular structure of the constituent material, or macroscopically, if Varuna has been loosely reassembled after fracturing by past impacts.

4. The high specific angular momentum of Varuna cannot have been supplied by collisions in the present-day, low-density trans-Neptunian belt. High H, leading to rotational deformation and binary formation, suggests an early, high-density phase in the trans-Neptunian belt. We infer an initial mass $M_i \sim 10$–$20\ M_\oplus$ from the apparently high incidence of binaries and rapidly rotating trans-Neptunian objects.

We thank John Dvorak and Paul deGrood for operating the UH telescope, Jane Luu, Yan Fernandez, and the anonymous referee for comments on the manuscript, and Fawad Chuhan for pointers about the literature of sand. This work was supported by a grant to D. C. J. from the National Science Foundation.

REFERENCES

Asphaug, E., & Benz, W. 1996, Icarus, 121, 225
Buie, M. W., Tholen, D. J., & Wasserman, L. H. 1997, Icarus, 125, 233
Carrier, W., Mitchell, J., & Mahmood, A. 1974, Geochim. Cosmochim. Acta Suppl., 5, 2361
Catullo, V., Zappalà, V., Farinella, P., & Paolicchi, P. 1984, A&A, 138, 464
Chandrasekhar, S. 1987, Ellipsoidal Figures of Equilibrium (New York: Dover)
Chuhan, F., Kjeldstad, A., & Bjørlykke, K. 2002, Marine and Petroleum Geology, in press
Dobrovolskis, A. R., Peale, S. J., & Harris, A. W. 1997, in Pluto and Charon, ed. S. A. Stern & D. J. Tholen (Tucson: Univ. Arizona Press), 159
Durham, W., Heard, H., & Kirby, S. 1983, J. Geophys. Res. Suppl., 88, 377
Dworetsky, M. M. 1983, MNRAS, 203, 917
Elliot, J. L., Kern, S. D., Osip, D. J., & Burles, S. M. 2001, IAU Circ. 7733
Farinella, P., & Davis, D. R. 1996, Science, 273, 938
Farinella, P., Paolicchi, P., Tedesco, E. F., & Zappalà, V. 1981, Icarus, 46, 114
Farnham, T. L. 2001, IAU Circ. 7583
Ida, S., Larwood, J., & Burkert, A. 2000, ApJ, 528, 351
Jewitt, D. C., Aussel, H., & Evans, A. 2001, Nature, 411, 446
Jewitt, D. C., & Luu, J. X. 2000, in Protostars and Planets IV, ed. V. Mannings, A. P. Boss, & S. S. Russell (Tucson: Univ. Arizona Press), 1201
———. 2001, AJ, 122, 2099
Jewitt, D. C., Luu, J. X., & Trujillo, C. 1998, AJ, 115, 2125
Jewitt, D. C., & Matthews, H. 1999, AJ, 117, 1056
Kavelaars, J., Petit, J.-M., Gladman, B., & Holman, M. 2001, IAU Circ. 7749
Kenyon, S. J., & Luu, J. X. 1999, AJ, 118, 1101
Knofel, A., & Stoss, R. 2000, Minor Planet Electron. Circ., No. 2000-Y45
Kossacki, K., & Leliwa-Kopystyński, J. 1993, Planet. Space Sci., 41, 729
Landolt, A. U. 1992, AJ, 104, 340
Leliwa-Kopystyński, J., Makkonen, L., Erikoinen, O., & Kossacki, K. 1994, Planet. Space Sci., 42, 545
Leone, G., Farinella, P., Paolicchi, P., & Zappalà, V. 1984, A&A, 140, 265
Lisse, C. M., A'Hearn, M. F., Hauser, M. G., Kelsall, T., Lien, D. J., Moseley, S. H., Reach, W. T., & Silverberg, R. F. 1998, ApJ, 496, 971
Love, S. G., & Ahrens, T. J. 1996, Icarus, 124, 141
Lupo, M., & Lewis, J. 1979, Icarus, 40, 157
Luu, J., & Jewitt, D. 1996, AJ, 112, 2310
McKinnon, W. B. 1989, ApJ, 344, L41
McMillan, R. S., & Larsen, J. A. 2000, Minor Planet Electron. Circ., No. 2000-X02
Millis, R. L. 1977, Icarus, 31, 81
Rickman, H. 1989, Adv. Space Res., 9(3), 59
Romanishin, W., Tegler, S. C., Rettig, T. W., Consolmagno, G., & Botthof, B. 2001, Proc. Natl. Acad. Sci., 98, 11863
Russell, H. 1906, ApJ, 24, 1
Sagdeev, R. Z., Elyasberg, P. E., & Moroz, V. I. 1988, Nature, 331, 240
Sheppard, S. S. 2001, IAU Circ. 7619
Sheppard, S. S., & Jewitt, D. C. 2002, AJ, submitted
Smith, B. A., et al. 1982, Science, 215, 504
———. 1986, Science, 233, 43
Stellingwerf, R. F. 1978, ApJ, 224, 953
Tholen, D. J., & Buie, M. W. 1997, in Pluto and Charon, ed. S. A. Stern & D. J. Tholen (Tucson: Univ. Arizona Press), 193
Trujillo, C. A., Jewitt, D. C., & Luu, J. X. 2001, AJ, 122, 457
Veillet, C. 2001, IAU Circ. 7610
Yeomans, D. K., et al. 1997, Science, 278, 2106
Young, E. F., Binzel, R. P., & Crane, K. 2001, AJ, 121, 552